ELECTROCHEMISTRY

Molecular origin of negative component of Helmholtz capacitance at electrified Pt(111)/water interface

Jia-Bo Le, Qi-Yuan Fan, Jie-Qiong Li, Jun Cheng*

Electrified solid/liquid interfaces are the key to many physicochemical processes in a myriad of areas including electrochemistry and colloid science. With tremendous efforts devoted to this topic, it is unexpected that molecular-level understanding of electric double layers is still lacking. Particularly, it is perplexing why compact Helmholtz layers often show bell-shaped differential capacitances on metal electrodes, as this would suggest a negative capacitance in some layer of interface water. Here, we report state-of-the-art ab initio molecular dynamics simulations of electrified Pt(111)/water interfaces, aiming at unraveling the structure and capacitive behavior of interface water. Our calculation reproduces the bell-shaped differential Helmholtz capacitance and shows that the interface water follows the Frumkin adsorption isotherm when varying the electrode potential, leading to a peculiar negative capacitive response. Our work provides valuable insight into the structure and capacitance of interface water, which can help understand important processes in electrocatalysis and energy storage in supercapacitors.

INTRODUCTION

An electric double layer (EDL) formed at an electrified interface can afford a potential change of a few volts within a very thin layer of 3 to 5 Å (*1*–*3*), amounting to an extremely large electric field of similar strength to that in a particle accelerator. Naturally, one would wonder how solvent molecules such as water or any other reactive species inside the EDL would behave in response to such a strong electric field. Answering this question is not only of fundamental interest but also of technological importance in a broad range of research areas in science and technology, to name a few, energy storage in supercapacitors (*4*, *5*), electrocatalysis of relevance to energy and environmental applications (*6*–*8*), self-assembly of colloidal particles (*9*), ion transport across biological membranes (*10*), and mineralization processes in earth science (*11*). Despite its significance, molecular-level understanding of EDL is largely missing, owing to its complexity and difficulty to probe. Because of the advent of advanced experimental (e.g., synchrotron-based techniques and Raman spectroscopy) and computational methods [e.g., ab intio molecular dynamics (AIMD) (*12*–*14*)], it is not until recently that the microscopic structures of EDL have started to be unveiled.

One of the key characteristics of EDL is its capacitance measuring the ratio of change in surface charge to potential change, which is accessible by conventional electrochemistry techniques such as voltammetry and impedance spectroscopy. The potential dependence of capacitance, i.e., differential capacitance, led to development of the well-known Gouy-Chapman-Stern (GCS) model of EDL, in which EDL consists of a Helmholtz (compact) layer and Gouy-Chapman (diffuse) layer, acting as two capacitors connected in series (see Fig. 1, A and B). The GCS theory, proposed about 100 years ago, successfully predicts the Gouy-Chapman minima in differential capacitance curves at the dilute limit (*15*) and remains as, yet, the main conceptual model for EDL. Among many others, one long standing puzzle is how to understand the bell-shaped differential capacitance curve of the Helmholtz layer (*15*, *16*). If representing the Helmholtz layer as capacitors in series, then it is inevitable to introduce negative capacitances for some of the layers (*17*, *18*). Although this is not excluded in principle, it is not satisfactory because of lack of physical underpinning. It was first noted in the 1970s by Trasatti that the Helmholtz capacitances of the simple *sp* metals correlate with their electronic densities (*19*). Since then, several theoretical models were proposed in attempts to relate this peculiar phenomenon with electronic effects of metal electrodes (*20*, *18*). For example, applying the jellium model to the *sp* metals, Schmickler (*18*) derived negative capacitances from change in surface potentials due to the response of electronic spillover to surface charges. Halley, Price, and colleagues (*17*, *21*) used first principles methods to calculate the capacitance curve of the Cu water interface.

Although insightful, these early attempts either completely ignored the metal lattice structures (*18*) or unrealistically represented the metal electronic structures, e.g., Cu pseudo-potential only treating *s* valence electrons (*21*), and, thus, cannot correctly describe the electronic interaction between metals and electrolyte solution. Starting from about three decades ago, chemisorption of molecules has been studied in great depth using new surface science techniques such as scanning tunneling microscopy (STM) and modern density functional theory (DFT) under ultrahigh vacuum conditions. For example, Michaelides and colleagues (*22*–*24*) studied the detailed microscopic structures of water monomers, clusters, and layers adsorbed on metal surfaces (e.g., Pt) by combining STM and DFT calculation. Very recently, state-of-the-art AIMD simulations have been applied to metal/water interfaces to calculate the interface structures and potentials (*25*–*33*). Notably, Cheng and colleagues (*25*) accurately computed the potentials of zero charge (PZC) of several transition metals and found that charge redistribution due to water chemisorption (see Fig. 1C) can induce substantial interface dipole potentials at PZC conditions, e.g., on the order of ~1 V on Pt (*34*). The question then arises: Will the water chemisorbed on metal surfaces contribute to the capacitative response of EDL when a bias is applied?

Aiming at unraveling the molecular origin of the Helmholtz capacitance, in this work, we perform extensive AIMD simulations of electrified Pt(111)/water interfaces and calculate the electrode

State Key Laboratory of Physical Chemistry of Solid Surfaces, iChEM, College of Chemistry and Chemical Engineering, Xiamen University, Xiamen 361005, China.
*Corresponding author. Email: chengjun@xmu.edu.cn

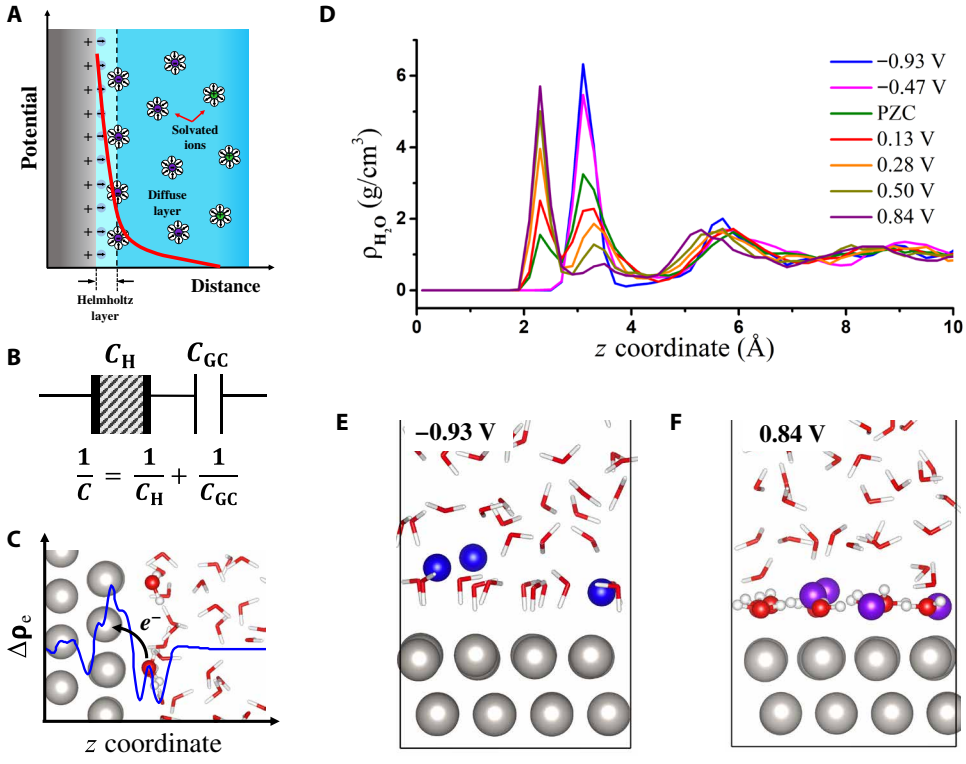

Fig. 1. Structure of electrified Pt(111)/water interface. (**A**) Schematic representation of the GCS model of the EDL. The EDL consists of a Helmholtz layer and Gouy-Chapman (diffuse) layer, and the interface potential distribution is shown by the red curve. (**B**) The EDL capacitance can be represented by the capacitors corresponding to the two layers (i.e., C_H and C_{GC}) connected in series. (**C**) Model of Pt(111)/water interface at PZC. There is significant interface electron redistribution along the surface normal *z* owing to water chemisorption, as indicated by the blue curve. (**D**) Profiles of water density (ρ_{H2O}) along the surface normal *z* at different potentials. The positions of water molecules are indicated by those of the oxygen atoms, and the zero in *z* coordinate indicates the position of the nuclei of the uppermost layer of Pt(111). All the potentials are referenced to the PZC of Pt(111). (**E** and **F**) Representative snapshots of the electrified Pt(111)/water interfaces at −0.93 and 0.84 V versus PZC. The Pt, Na, F, O, and H atoms are colored in gray, blue, violet, red, and white, respectively. The chemisorbed water is highlighted with the ball-and-stick model in comparison to other water with the stick model.

potentials using the recently developed computational standard hydrogen electrode (cSHE) method as a function of surface charge densities. We reproduce the bell-shaped differential capacitance curve, and detailed analyses show that the surface coverage of chemisorbed water can vary with the applied potential. Our calculation demonstrates that the adsorption/desorption processes of surface water with varying potentials give rise to the negative component of the Helmholtz capacitance. We further propose a theoretical model based on the Frumkin adsorption isotherm that can well describe our calculated results. Our work highlights the importance of the molecular-level picture and electronic structure of EDL for understanding the capacitive behavior of the interface water.

RESULTS

Structure of interface water

As illustrated in fig. S1, a series of electrified Pt(111)/water interface models have been built at different surface charge densities (σ), in which the surface charges are compensated by counter ions, i.e., Na^+ or F^-, located at the outer Helmholtz planes. Note that our EDL models do not account for the Gouy-Chapman layer and, therefore, correspond to high concentration conditions.

The simulation cells are kept charge neutral, and the surface charge densities are controlled by the number of counter ions added in the cells. Detailed descriptions on the models are given in Materials and Methods section, and charge distribution plots in fig. S2 show where the charges are located at the electrified interfaces. These models are simulated using AIMD for first equilibration and then production of data, and the corresponding electrode potentials versus SHE can be obtained from these AIMD trajectories using the cSHE method [see the Supplementary Materials and (*25*, *35*, *36*) for detailed explanation on the methodology]. We have successfully applied the same method to the Au(111)/water interface for elucidating the molecular structure of water inside the Helmholtz layer at negative bias (*12*).

These models cover a potential window ranging from −0.93 to 0.84 V with respect to the PZC of Pt(111) [i.e., 0.2 to 0.3 V versus SHE (*25*, *37*–*40*)], which enables us to investigate the water structure and capacitance of the Helmholtz layer on Pt(111). It is worth mentioning that, in this work, we ignore the specific adsorption of H and OH, which amounts to the pH conditions when specific adsorption is insignificant, and the experimental capacitances we compare against are removed with pseudo-capacitances due to specific adsorption (*41*–*43*).

Detailed analyses of the AIMD trajectories show that the density and orientation of the interface water are strongly dependent on the applied potential and the profiles of water density (ρ_{H2O}) and orientation distribution, indicated by the angle φ between the bisector of

water and the surface normal and the angle θ between the O—H bond of water and the surface normal, are illustrated in Fig. 1 and Fig. 2 (A and B), respectively. Note from the density profiles that there are two distinct peaks of interface water in the Helmholtz layer ($z < \sim 4$ Å, where z is the distance from the surface); one peak at z = 2.3 Å corresponds to the water directly chemisorbed on the surface, and the other at z = 3.3 Å represents the nonchemisorbed water in the Helmholtz layer. This finding of two layers of interface water is also in line with the understanding from the work of Feliu and co-workers (*44*) on Pt(111). At the very negative potential of −0.93 V, there is no water chemisorbed on the surface due to Coulombic repulsion, and thereby, the first peak at z = 2.3 Å disappears. All the water molecules in the Helmholtz layer take a "one-H-down" configuration with one hydrogen atom pointing to the metal surface (see Fig. 1E), and the hydrogen bond analysis shown in Fig. 2C indicates that the other hydrogen of the one-H-down water forms a hydrogen bond with the neighboring water, similar to those observed on Au(111) at negative bias (*12*). This type of water features φ peaked at ~135° and θ at ~90° and ~165° in the orientation distribution profile of Fig. 2 (A and B). As the potential increases, the interface water starts to adsorb on the surface, leading to gradual increase in the intensity of the first peak and decrease in the second peak at z = 3.3 Å in the water density profile of Fig. 1D. At the very positive potential of 0.84 V, almost all the water molecules in the Helmholtz layer are chemisorbed on the surface, approaching to the saturated coverage of ~0.5 monolayer (ML). As shown in Fig. 1F and Fig. 2 (A and B), the chemisorbed water sits on the top site of Pt(111), with its molecular plane nearly paralleled to the surface and two hydrogen atoms slightly tilting up, and the orientation takes φ peaked at ~60° and both θ at ~75°. Moreover, it is revealed from Fig. 2C that at very positive potentials, each chemisorbed water accepts approximately one hydrogen bond from the neighboring chemisorbed water, indicating the formation of a two-dimensional (2D) hydrogen bond network on Pt(111). The 2D hydrogen bond network benefits from the matching of the hydrogen bonds between chemisorbed water and the underlying Pt lattice (both being ~2.8 Å) and helps stabilize the structure of chemisorbed water at positive potentials.

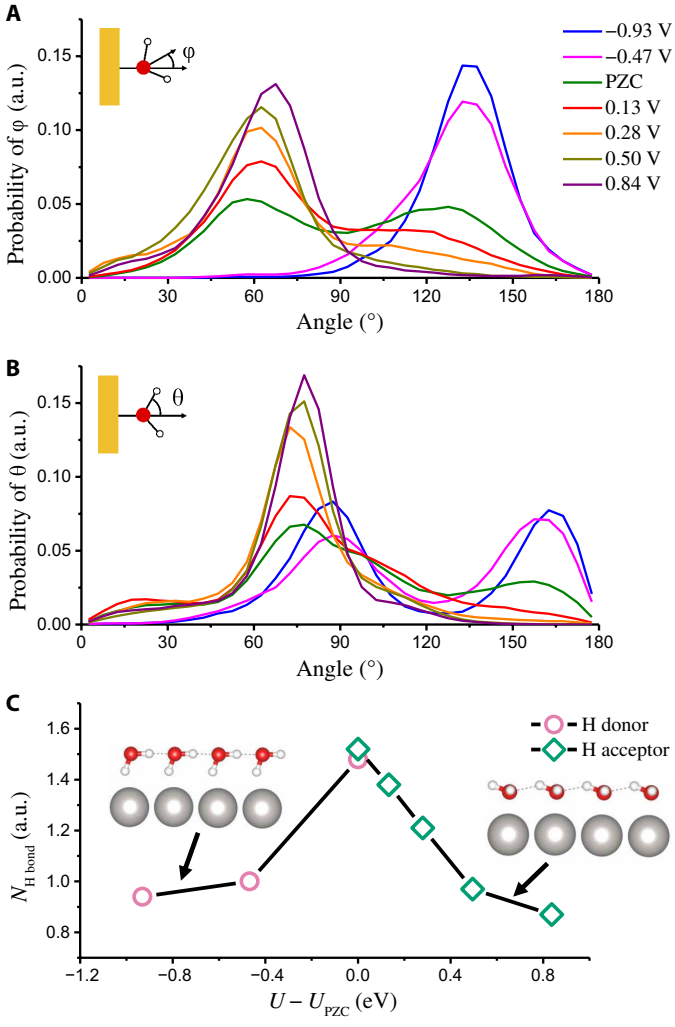

Fig. 2. Orientation and hydrogen bonding of interface water. Probability distribution profiles of angle φ (**A**) between the bisector of water and the surface normal and angle θ (**B**) between the O—H bond of water and the surface normal of the interface water at different applied potentials. Both angles are shown in the insets, and the interface water is taken as being within 4 Å˚ from the metal surface. The potentials are referenced to the PZC of Pt(111). (**C**) Number of hydrogen bond donors (pink circle) and acceptors (green diamond) of interface water molecules as a function of potential. A hydrogen bond is defined when the O—O distance is shorter than 3.5 Å and the O—O—H angle is less than 35°. The insets show the structural models of interface water at very negative and positive potentials. a.u., arbitrary units.

Capacitance of interface water

As mentioned above, a small fraction of ML of chemisorbed water at PZC can induce a significant interface potential (~1 V) on Pt (*25*, *45*, *46*). It can, thus, be conceived that the observed potential dependence of surface coverage of chemisorbed water may have direct impact on the capacitive response of interface water. A simple model in Fig. 3 can be proposed to demonstrate this effect. The interface potential change (Δψ) across the Helmholtz layer can be decomposed into two parts, namely, the usual potential change induced by the surface charge ($\Delta\psi_{sol}$) and the potential due to water chemisorption ($\Delta\psi_A$). At PZC, the surface charge is zero, and thus, $\Delta\psi_{sol} = 0$. Whereas, there is a remaining contribution from $\Delta\psi_A$ due to water chemisorption (see Fig. 3B) (*25*). Since the electron density transfers from water to Pt, $\Delta\psi_A$ will lead to a negative shift of the electrode potential. At a potential much more negative than PZC (Fig. 3A), all chemisorbed water desorbs from the surface, indicating that $\Delta\psi_A = 0$ and only $\Delta\psi_{sol}$ contributes to the overall Δψ. At a potential more positive than PZC (Fig. 3C), both $\Delta\psi_{sol}$ and $\Delta\psi_A$ are finite but with opposite signs and, thus, compensate each other to give a smaller overall Δψ. This qualitative analysis shows that involving the $\Delta\psi_A$ term due to chemisorbed water can give a smaller potential change and, thus, an increased capacitance. When the surface charge changes from negative to positive, more water is adsorb on the surface, and $\Delta\psi_A$ shifts to more negative (opposite to $\Delta\psi_{sol}$), thereby implying a negative capacitance.

To further show a quantitative picture, we plot the surface charge density σ and the coverage of chemisorbed water θ_A as a function of the electrode potential U, as illustrated in Fig. 4. It is clear that the σ − U plot is nonlinear and shows an S-shaped relation, which implies a bell-shaped differential capacitance C_H of the Helmholtz layer. The θ_{A-U} plot is also S-shaped, which is familiar from adsorption isotherms. Since chemisorbed water can induce interface dipole and, thus, must repel with each other, the water adsorption/desorption

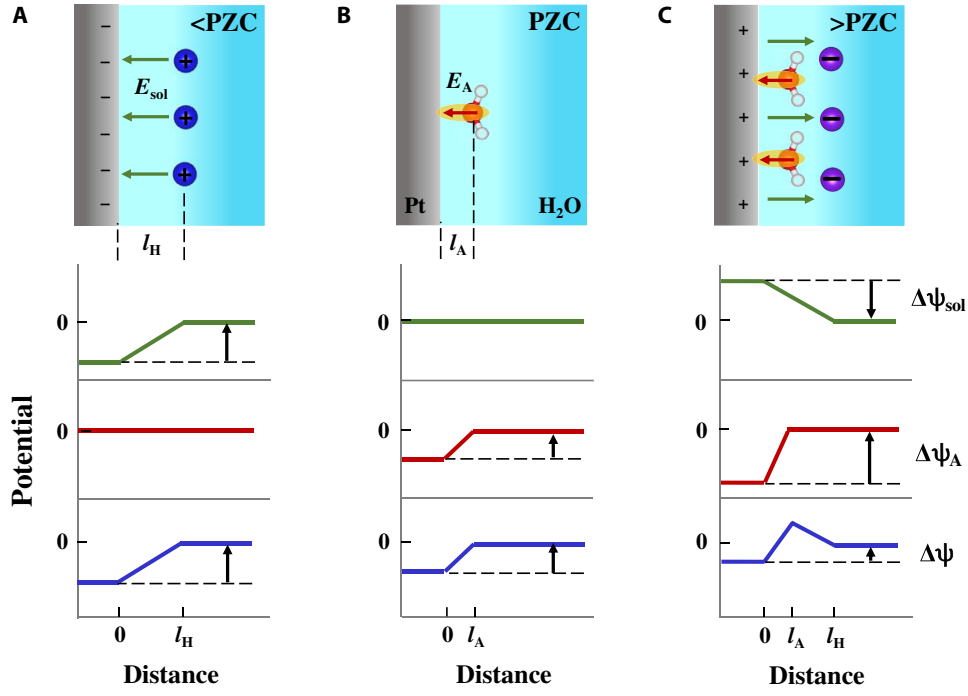

Fig. 3. Proposed model of Helmholtz layer. Potential profiles at the Pt(111)/water interface at different applied potentials (**A**) <PZC without water chemisorption, (**B**) PZC, and (**C**) >PZC. The Pt electrode and water solution are the regions colored by gray and light blue, respectively. The balls in red, white, blue, and violet stand for oxygen atoms, hydrogen atoms, cations, and anions, respectively. The interface potential change $\Delta\psi$ (blue) consists of the usual potential change $\Delta\psi_{sol}$ induced by the surface charge (green) and the potential $\Delta\psi_A$ caused by water chemisorption (red). The potential in bulk solution is set to zero. l_A and l_H denote the distance separation of the dipole induced by chemisorbed water and Helmholtz layer, respectively.

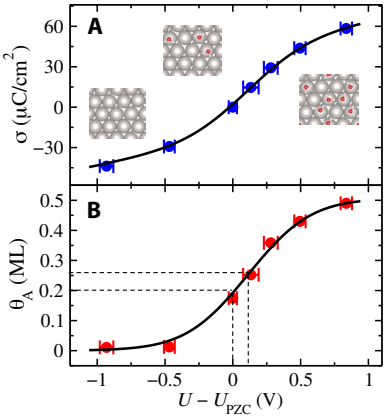

Fig. 4. AIMD data and model fitting. Plots of surface charge density σ (**A**) and surface coverage of chemisorbed water θ_A (**B**) as a function of the electrode potential *U*. The solid dots with error bars represent the computed data from AIMD simulations, and the black curves are the corresponding fits using the proposed theoretical model. The convergence of the computed *U* and the corresponding θ_A can found in figs. S3 and S7. The insets in (A) show the representative configurations of the chemisorbed water on Pt(111) at −0.93 V, PZC, and 0.84 V, respectively. The dashed lines in (B) indicate the respective θ_A at PZC and ~0.1 V. The potentials are referenced to the PZC (U_{PZC}).

process upon charging would follow the Frumkin adsorption isotherm (*47*). We thus adopt this isotherm to formulate the capacitative behavior of the Helmholtz layer on Pt, and detailed derivation of the relations of σ, *U*, and θ_A is given in the Supplementary Materials. In our formalism, we assume that the electronic dipole of chemisorbed water is independent of the electrode potential, but note that the chemisorption-induced dipole should be generally polarizable in the presence of an electric field (*48*). The polarizable effect, however, is small in our case, and moreover, the electric field due to surface charge is compensated by the lateral dipole-dipole interaction between chemisorbed water (see section S4).

As can be seen in Fig. 4 and fig. S8, the fitted curves (black) can very well describe the computed data. On the basis of the fitted curves, we find that C_H shows a maximum of ~100 μF/cm^2 at a potential slightly more positive (~0.1 V) than the PZC, and it decays to ~20 μF/cm^2 when the electrode potential moves away from the PZC. Most of the features of the C_H (blue curve in Fig. 5) are very similar to the experimental differential capacitance curves (*41*–*43*). It is worth mentioning that the comparison is more informative near the double layer region as, for example, significant specific adsorption of H outside this region could result in narrowing of the C_H peak (*42*).

We also derive a theoretical model consisting of two capacitors in series for representing the Helmholtz capacitance (C_H). In this model, one component, denoted by C_{sol}, corresponds to the usual dielectric response of solvent in the Helmholtz layer, and the fitted value is ~20 μF/cm^2, closely resembling the Helmholtz capacitance on inert metals such as Hg. The other component C_A accounts for the effect of water chemisorption. The obtained value of C_A is negative, with the maximum around the PZC, as shown in Fig. 5. Connecting the two capacitors (C_{sol} and C_A) can give rise to the bell-shaped profile of C_H. From the formula of C_A (i.e., eq. S16), we note that C_A reaches maximum when the θ_A is equal to the half of the maximum

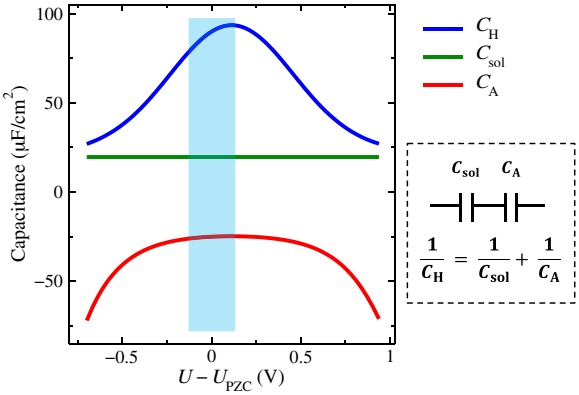

Fig. 5. Capacitance of the Helmholtz layer. Decomposition of differential Helmholtz capacitance C_H (blue) as a function of electrode potential U into two constituent components, the solvent capacitance C_{sol} (green) and the capacitance C_A (red) due to water chemisorption. The inset indicates that C_{sol} and C_A are connected in series. The potential window (~0.2 V) of the double layer region of the Pt(111)/water interface at pH 4 is highlighted by light blue (*38*).

coverage of the chemisorbed water on Pt(111), i.e., ~0.25 ML. As shown in Fig. 4B, the corresponding potential is ~0.1 V versus PZC, and the θ_A at PZC is ~0.16 ML. This explains why the potential corresponding to the C_H maximum is slightly more positive than the PZC on Pt (*41*, *42*).

DISCUSSION

Our calculation and proposed model clearly show that the peak of differential capacitance C_H is caused by water chemisorption, leading to a negative capacitance C_A. The magnitude of the latter depends strongly on the dipole of chemisorbed water on the metal surface (see eq. S10) and, thus, the binding strength of water. This may help rationalize the trend of the Helmholtz capacitance on other transition metals [e.g., Au and Ag (*49*, *50*)] and sd metals [e.g., Hg (*15*)]; for example, the maximum of C_H on Pt is more pronounced than those on Au and Hg. Moreover, our results suggest that incorporation of solvent chemisorption on electrodes could offer a new strategy for enhancing the double layer capacitance for energy storage in supercapacitors. Our new model also reveals detailed changes in solvation environment at interfaces under different potentials, which would be of close relevance to electrocatalytic reactions (e.g., hydrogen evolution, oxygen reduction, and CO_2 reduction) occurring inside the Helmholtz layers.

To summarize, we investigate the Helmholtz layer at the Pt(111)/water interfaces at different potential conditions using AIMD calculation. The focus is to reveal the molecular structure of interface water and the response to the electric field in the Helmholtz layer. We find that the surface coverage of chemisorbed water increases when shifting the potential from negative to positive. As chemisorbed water can induce a significant interface dipole potential, change in its coverage will lead to a potential change and, hence, a negative capacitive response. Combining with the normal dielectric response of the solvent, we can obtain the experimentally observed bell-shaped differential capacitance of the Helmholtz layer. Our work demonstrates the importance of water chemisorption on metal electrodes to the EDL capacitance and, thus, sheds new light on the relationship between the molecular structure and capacitative behavior of interface water. Furthermore, our finding lays the foundation for future exploration of tuning electronic interactions between electrodes and electrolyte solutions for optimizing the performances of energy materials in electrocatalysis and supercapacitors.

MATERIALS AND METHODS

Models of electrified Pt(111)/water interfaces

The Pt(111) surface was modeled with a $p(4 \times 4)$ periodic slab of four atomic layers. The vacuum space between the slab and its periodic images is 21 Å and fully filled with water molecules. The cell contains 64 Pt atoms and 68 water molecules with the size of 11.246 Å × 11.246 Å × 27.887 Å. The metal work function and the PZC of this model, as reported in (*25*), are close to the experimental values (*38*–*40*, *51*). The electrified Pt(111)/H_2O interfaces were modeled by inserting Na^+ or F^- ions near the Pt(111) surface. Note that Na^+ and F^- ions do not specifically adsorb on Pt(111), thus forming the outer Helmholtz plane, and at the time scale of AIMD, these ions do not diffuse away into the bulk water. All the models are charge neutral, and the electronic structures of the interfaces are optimized to generate double layers with ions and charged surfaces with opposite signs. The charges of ions in the models are evidenced by the calculated projected density of states, as shown in fig. S5. Varying the number of Na^+ or F^- in the model amounts to controlling the surface charge density and, hence, the electrode potential. Using this approach, six electrified Pt(111)/water interfaces were constructed with the surface charge density of −43.8, −29.2, 14.6, 29.2, 43.8, and 58.4 μC/cm^2. The densities of the bulk water in these models were kept close to 1 g/cm^3. These models contain two symmetrical interfaces, and therefore, the net dipoles of these models are canceled, as illustrated in the averaged electrostatic potential profiles in fig. S4. The electrode potentials of the electrified interface models were calculated with the cSHE method (*25*). Note that Gouy-Chapman layers are not included in the interface models, and thus, our EDL models correspond to the high concentration limit where the surface charges are effectively screened within the Helmholtz layer. Co-ions are also omitted in our models, which may not affect our study on the water structure and capacitance of the Helmholtz layer since our EDL models have the correct charge excess. It is worth mentioning that the same model setup was successfully used in elucidating the structure of the Helmholtz layer on Au (*12*).

Computational setup

The AIMD simulations were performed using the freely available CP2K/Quickstep package (*52*). The DFT implemented in CP2K is based on a hybrid Gaussian plane wave scheme. The orbitals are described by an atom-centered Gaussian-type basis set, and an auxiliary plane wave basis set is used to reexpand the electron density in the reciprocal space. The 2s and 2p electrons of O; 2s, 2p, and 3s electrons of Na; 2s and 2p electrons of F; and 5d and 6s electrons of Pt are treated as valence, and the rest core electrons were represented by Goedecker-Teter-Hutter pseudo-potentials (*53*, *54*). The Gaussian basis sets were double ζ with one set of polarization functions (*55*), and the energy cutoff was set to 400 rydbergs. We used the Perdew-Burke-Ernzerhof functional (*56*) to describe exchange-correlation effects, and the dispersion correction was applied in all calculations with the Grimme D3 method (*57*). Because of the large size of the cells, only the Γ point in the reciprocal space was used in our calculations.

The second-generation Car-Parrinello molecular dynamics (SGCP-MD) (*58*, *59*) was used for sampling structures of the interface models, and the target temperature was set to 330 K. The correction step was obtained by five iterations of the orbital transformation optimization (*60*), and the integration time for each step was 0.5 fs. The Langevin friction coefficient (γ_L) was set to 0.001 fs^{-1}, and the intrinsic friction coefficient (γ_D) was varied, i.e., 5×10^5 fs^{-1} for Pt and 2.2×10^4 fs^{-1} for H_2O and ions. More details on the SGCPMD setup can be found in (*59*). For each AIMD simulation, an initial ~5 ps (~10,000 steps) of molecular dynamics trajectory was used to equilibrate the system and then followed by a production period of more than 15 ps.

SUPPLEMENTARY MATERIALS

Supplementary material for this article is available at http://advances.sciencemag.org/cgi/content/full/6/41/eabb1219/DC1

REFERENCES AND NOTES

1. J. O. Bockris, B. E. Conway, E. Yeager, *Comprehensive Treatise of Electrochemistry: The Double Layer* (Plenum Press, 1980).
2. W. Schmickler, R. Guidelli, The partial charge transfer. *Electrochim. Acta* **127**, 489–505 (2014).
3. B. E. Conway, *Modern Aspects of Electrochemistry. No. 38* (Kluwer Academic/Plenum Publishers, 2005).
4. C. Merlet, B. Rotenberg, P. A. Madden, P.-L. Taberna, P. Simon, Y. Gogotsi, M. Salanne, On the molecular origin of supercapacitance in nanoporous carbon electrodes. *Nat. Mater.* **11**, 306–310 (2012).
5. M. Salanne, B. Rotenberg, K. Naoi, K. Kaneko, P.-L. Taberna, C. P. Grey, B. Dunn, P. Simon, Efficient storage mechanisms for building better supercapacitors. *Nat. Energy* **1**, 16070 (2016).
6. H. S. Casalongue, S. Kaya, V. Viswanathan, D. J. Miller, D. Friebel, H. A. Hansen, J. K. Nørskov, A. Nilsson, H. Ogasawara, Direct observation of the oxygenated species during oxygen reduction on a platinum fuel cell cathode. *Nat. Commun.* **4**, 2817 (2013).
7. J. K. Nørskov, J. Rossmeisl, A. Logadottir, L. Lindqvist, J. R. Kitchin, T. Bligaard, H. Jónsson, Origin of the overpotential for oxygen reduction at a fuel-cell cathode. *J. Phys. Chem. B* **108**, 17886–17892 (2004).
8. I. Ledezma-Yanez, W. D. Z. Wallace, P. Sebastián-Pascual, V. Climent, J. M. Feliu, M. T. M. Koper, Interfacial water reorganization as a pH-dependent descriptor of the hydrogen evolution rate on platinum electrodes. *Nat. Energy* **2**, 17031 (2017).
9. Y. Yang, G. Chen, S. Thanneeru, J. He, K. Liu, Z. Nie, Synthesis and assembly of colloidal cuboids with tunable shape biaxiality. *Nat. Commun.* **9**, 4513 (2018).
10. M. P. Grzelczak, S. P. Danks, R. C. Klipp, D. Belic, A. Zaulet, C. Kunstmann-Olsen, D. F. Bradley, T. Tsukuda, C. Viñas, F. Teixidor, J. J. Abramson, M. Brust, Ion transport across biological membranes by carborane-capped gold nanoparticles. *ACS Nano* **11**, 12492–12499 (2017).
11. J. J. De Yoreo, P. U. P. A. Gilbert, N. A. J. M. Sommerdijk, R. L. Penn, S. Whitelam, D. Joester, H. Zhang, J. D. Rimer, A. Navrotsky, J. F. Banfield, A. F. Wallace, F. M. Michel, F. C. Meldrum, H. Cölfen, P. M. Dove, Crystallization by particle attachment in synthetic, biogenic, and geologic environments. *Science* **349**, aaa6760 (2015).
12. C.-Y. Li, J.-B. Le, Y.-H. Wang, S. Chen, Z.-L. Yang, J.-F. Li, J. Cheng, Z.-Q. Tian, In situ probing electrified interfacial water structures at atomically flat surfaces. *Nat. Mater.* **18**, 697 (2019).
13. J.-J. Velasco-Velez, C. H. Wu, T. A. Pascal, L. F. Wan, J. Guo, D. Prendergast, M. Salmeron, The structure of interfacial water on gold electrodes studied by x-ray absorption spectroscopy. *Science* **346**, 831–834 (2014).
14. Y. Tong, F. Lapointe, M. Thämer, M. Wolf, R. K. Campen, Hydrophobic water probed experimentally at the gold electrode/aqueous interface. *Angew. Chem. Int. Ed.* **56**, 4211–4214 (2017).
15. W. Schmickler, E. Santos, *Interfacial Electrochemistry* (Springer, ed. 2, 2010).
16. J. Huang, T. Zhou, J. Zhang, M. Eikerling, Double layer of platinum electrodes: Non-monotonic surface charging phenomena and negative double layer capacitance. *J. Chem. Phys.* **148**, 044704 (2018).
17. J. W. Halley, A. Mazzolo, Y. Zhou, D. Price, First-principles simulations of the electrode–electrolyte interface. *J. Electroanal. Chem.* **450**, 273–280 (1998).
18. W. Schmickler, Electronic effects in the electric double layer. *Chem. Rev.* **96**, 3177–3200 (1996).
19. H. Gerischer, C. W. Tobias, *Advances in Electrochemistry and Electrochemical Engineering* (Wiley Interscience, 1977).
20. A. A. Kornyshev, Metal electrons in the double layer theory. *Electrochim. Acta* **34**, 1829–1847 (1989).
21. S. Walbran, A. Mazzolo, J. W. Halley, D. L. Price, Model for the electrostatic response of the copper-water interface. *J. Chem. Phys.* **109**, 8076–8080 (1998).
22. A. Michaelides, V. A. Ranea, P. L. de Andres, D. A. King, General model for water monomer adsorption on close-packed transition and noble metal surfaces. *Phys. Rev. Lett.* **90**, 216102 (2003).
23. J. Carrasco, A. Hodgson, A. Michaelides, A molecular perspective of water at metal interfaces. *Nat. Mater.* **11**, 667–674 (2012).
24. A. Michaelides, K. Morgenstern, Ice nanoclusters at hydrophobic metal surfaces. *Nat. Mater.* **6**, 597–601 (2007).
25. J. Le, M. Iannuzzi, A. Cuesta, J. Cheng, Determining potentials of zero charge of metal electrodes versus the standard hydrogen electrode from based on density-functional-theory-based molecular dynamics. *Phys. Rev. Lett.* **119**, 016801 (2017).
26. A. Bouzid, A. Pasquarello, Atomic-scale simulation of electrochemical processes at electrode/water interfaces under referenced bias potential. *J. Phys. Chem. Lett.* **9**, 1880–1884 (2018).
27. S. Sakong, A. Groß, The electric double layer at metal-water interfaces revisited based on a charge polarization scheme. *J. Chem. Phys.* **149**, 084705 (2018).
28. A. Bagger, L. Arnarson, M. H. Hansen, E. Spohr, J. Rossmeisl, Electrochemical CO reduction: A property of the electrochemical interface. *J. Am. Chem. Soc.* **141**, 1506–1514 (2019).
29. J. Rossmeisl, E. Skúlason, M. E. Björketun, V. Tripkovic, J. K. Nørskov, Modeling the electrified solid–liquid interface. *Chem. Phys. Lett.* **466**, 68–71 (2008).
30. M. Otani, I. Hamada, O. Sugino, Y. Morikawa, Y. Okamoto, T. Ikeshoji, Structure of the water/platinum interface - A first principles simulation under bias potential. *Phys. Chem. Chem. Phys.* **10**, 3609–3612 (2008).
31. S. Schnur, A. Groß, Properties of metal-water interfaces studied from first principles. *New J. Phys.* **11**, 125003 (2009).
32. H. H. Kristoffersen, T. Vegge, H. A. Hansen, OH formation and H_2 adsorption at the liquid water-Pt(111) interface. *Chem. Sci.* **9**, 6912–6921 (2018).
33. T. Cheng, L. Wang, B. V. Merinov, W. A. Goddard III, Explanation of dramatic pH-dependence of hydrogen binding on noble metal electrode: Greatly weakened water adsorption at high pH. *J. Am. Chem. Soc.* **140**, 7787–7790 (2018).
34. R. Jinnouchi, A. B. Anderson, Electronic structure calculations of liquid-solid interfaces: Combination of density functional theory and modified Poisson-Boltzmann theory. *Phys. Rev. B* **77**, 245417 (2008).
35. J. Cheng, M. Sprik, Alignment of electronic energy levels at electrochemical interfaces. *Phys. Chem. Chem. Phys.* **14**, 11245–11267 (2012).
36. J. Cheng, X. Liu, J. VandeVondele, M. Sulpizi, M. Sprik, Redox potentials and acidity constants from density functional theory based molecular dynamics. *Acc. Chem. Res.* **47**, 3522–3529 (2014).
37. R. Martínez-Hincapié, V. Climent, J. M. Feliu, Peroxodisulfate reduction as a probe to interfacial charge. *Electrochem. Commun.* **88**, 43–46 (2018).
38. R. Rizo, E. Sitta, E. Herrero, V. Climent, J. M. Feliu, Towards the understanding of the interfacial pH scale at Pt(111) electrodes. *Electrochim. Acta* **162**, 138–145 (2015).
39. K. Ojha, N. Arulmozhi, D. Aranzales, M. T. M. Koper, Double layer of Pt(111)-aqueous electrolyte interface: Potential of zero charge and anomalous Gouy-Chapman screening. *Angew. Chem. Int. Ed.* **59**, 711–715 (2019).
40. A. Cuesta, Measurement of the surface charge density of CO-saturated Pt(111) electrodes as a function of potential: The potential of zero charge of Pt(111). *Surf. Sci.* **572**, 11–22 (2004).
41. T. Pajkossy, D. Kolb, On the origin of the double layer capacitance maximum of Pt(111) single crystal electrodes. *Electrochem. Commun.* **5**, 283–285 (2003).
42. T. Pajkossy, D. Kolb, Double layer capacitance of Pt(111) single crystal electrodes. *Electrochim. Acta* **46**, 3063–3071 (2001).
43. N. Garcia-Araez, V. Climent, E. Herrero, J. M. Feliu, J. Lipkowski, Thermodynamic approach to the double layer capacity of a Pt(111) electrode in perchloric acid solutions. *Electrochim. Acta* **51**, 3787–3793 (2006).
44. A. Berná, V. Climent, J. M. Feliu, New understanding of the nature of OH adsorption on Pt(111) electrodes. *Electrochem. Commun.* **9**, 2789–2794 (2007).
45. J. Le, A. Cuesta, J. Cheng, The structure of metal-water interface at the potential of zero charge from density functional theory-based molecular dynamics. *J. Electroanal. Chem.* **819**, 87–94 (2018).
46. J. Le, Q. Fan, L. Perez-Martinez, A. Cuesta, J. Cheng, Theoretical insight into the vibrational spectra of metal-water interfaces from density functional theory based molecular dynamics. *Phys. Chem. Chem. Phys.* **20**, 11554–11558 (2018).
47. E. Gileadi, *Physical Electrochemistry. Fundamentals, Techniques and Applications* (Wiley-VCH, 2011).
48. A. Kopač Lautar, A. Hagopian, J.-S. Filhol, Modeling interfacial electrochemistry: Concepts and tools. *Phys. Chem. Chem. Phys.* **22**, 10569–10580 (2020).
49. T. Pajkossy, T. Wandlowski, D. M. Kolb, Impedance aspects of anion adsorption on gold single crystal electrodes. *J. Electroanal. Chem.* **414**, 209–220 (1996).

50. G. Valette, Double layer on silver single crystal electrodes in contact with electrolytes having anions which are slightly specifically adsorbed: Part III. The (111) face. *J. Electroanal. Chem.* **269**, 191–203 (1989).
51. H. B. Michaelson, The work function of the elements and its periodicity. *J. Appl. Phys.* **48**, 4729 (1977).
52. J. VandeVondele, M. Krack, F. Mohamed, M. Parrinello, T. Chassaing, J. Hutter, QUICKSTEP: Fast and accurate density functional calculations using a mixed Gaussian and plane waves approach. *Comput. Phys. Commun.* **167**, 103–128 (2005).
53. S. Goedecker, M. Teter, J. Hutter, Separable dual-space Gaussian pseudopotentials. *Phys. Rev. B* **54**, 1703 (1996).
54. C. Hartwigsen, S. Goedecker, J. Hutter, Relativistic separable dual-space Gaussian pseudopotentials from H to Rn. *Phys. Rev. B* **58**, 3641 (1998).
55. J. VandeVondele, J. Hutter, Gaussian basis sets for accurate calculations on molecular systems in gas and condensed phases. *J. Chem. Phys.* **127**, 114105 (2007).
56. J. P. Perdew, K. Burke, M. Ernzerhof, Generalized gradient approximation made simple. *Phys. Rev. Lett.* **77**, 3865 (1996).
57. S. Grimme, J. Antony, S. Ehrlich, H. Krieg, A consistent and accurate ab initio parametrization of density functional dispersion correction (DFT-D) for the 94 elements H-Pu. *J. Chem. Phys.* **132**, 154104 (2010).
58. T. D. Kühne, M. Krack, F. R. Mohamed, M. Parrinello, Efficient and accurate Car-Parrinello-like approach to Born-Oppenheimer molecular dynamics. *Phys. Rev. Lett.* **98**, 066401 (2007).
59. J. Lan, J. Hutter, M. Iannuzzi, First-principles simulations of an aqueous CO/Pt(111) interface. *J. Phys. Chem. C* **122**, 24068–24076 (2018).
60. J. VandeVondele, J. Hutter, An efficient orbital transformation method for electronic structure calculations. *J. Chem. Phys.* **118**, 4365–4369 (2003).

Acknowledgments: We thank J. Lan and M. Iannuzzi for technical support on CP2K and setup of the SGCPMD, and J. Feliu, M. T. M. Koper, J. Lipkowski, and C. Amatore for helpful discussion. **Funding:** J.C. is grateful for funding support by the National Natural Science Foundation of China (grant nos. 21991151, 21861132015, and 21621091) and the Principal's Fund of Xiamen University (20720190047). J.-B.L. thanks for the funding from the National Natural Science Foundation of China (grant no. 21902136) and the China Postdoctoral Science Foundation (2018M642563). **Author contributions:** J.C. and J.-B.L. conceived and designed the project and wrote the manuscript. J.-B.L. performed the calculation, and J.-B.L., J.C., Q.-Y.F., and J.-Q.L. analyzed the results. **Competing interests:** The authors declare that they have no competing interests. **Data and materials availability:** All data needed to evaluate the conclusions in the paper are present in the paper and/or the Supplementary Materials. Additional data related to this paper may be requested from the authors.

Submitted 1 February 2020
Accepted 20 August 2020
Published 7 October 2020
10.1126/sciadv.abb1219

Citation: J.-B. Le, Q.-Y. Fan, J.-Q. Li, J. Cheng, Molecular origin of negative component of Helmholtz capacitance at electrified Pt(111)/water interface. *Sci. Adv.* **6**, eabb1219 (2020).

Molecular origin of negative component of Helmholtz capacitance at electrified Pt(111)/water interface

Jia-Bo Le, Qi-Yuan Fan, Jie-Qiong Li and Jun Cheng

Sci Adv **6** (41), eabb1219.
DOI: 10.1126/sciadv.abb1219